Optimization of a material with a negative stiffness provided by an inherent bistable element

J. Heczko
European Centre of Excellence, NTIS - New Technologies for Information Society, Faculty of Applied Sciences, University of West Bohemia, Pilsen, Czech Republic

Z. Dimitrovová
Departamento de Engenharia Civil, Faculdade de Ciências e Tecnologia, Universidade Nova de Lisboa and LAETA, IDMEC, Instituto Superior Técnico, Universidade de Lisboa, Lisboa, Portugal

H.C. Rodrigues
LAETA, IDMEC, Instituto Superior Técnico, Universidade de Lisboa, Lisboa, Portugal

ABSTRACT: It is known from literature that extreme damping can be achieved in materials incorporating negative stiffness inclusions. In this paper a material realization of such a structure is presented and its behaviour is analysed. Polyethylene foam sheets are utilized as a base material and a negative stiffness component is supplied by an inherent bistable element introduced with the help of curved cuts. The damping performance can be optimized by a shape optimization provided a reliable finite element model is available. This paper gives guidelines to material fitting of such a structure, namely two methods are presented and a suitable material model is identified. The work presented is done in continuation of Heczko et al. (in press).

1 INTRODUCTION

Recent interest in material design optimization can be attributed to the significant progress in material processing. Material properties can be tailored by optimization techniques to achieve an optimal response to a given solicitation, which serves as an input to the development of new materials, unavailable in nature. It has already been proven that extreme stiffness and damping can be achieved in materials incorporating negative stiffness inclusions (Jaglinski et al. 2007, Lakes 2001). Nevertheless, material realization in this regard is still a challenging task (Kashdan et al. 2012, Kalathur & Lakes 2013).

In this paper a polyethylene foam sheets are utilized as a base material for a structure exhibiting a negative stiffness over a finite range of global strains. The negative stiffness is supplied by an inherent bistable element introduced with the help of curved cuts. It was verified experimentally that such a material exhibits a negative stiffness branch in the effective force displacement graph, over a finite range of displacement, under a displacement control uniaxial tension test.

In order to optimize such a material with regard to vibration damping, several geometrical parameters describing the position and size of these additional cuts have to be taken into account. This optimization can be accomplished within a finite element model and, at the same time, with the help of a simple discrete mechanism. The procedure of obtaining the discrete mechanism is described in Heczko et al. (in press). The main advantage of this representation is that the mechanism dynamic behaviour characteristics can be solved analytically. Then the optimization can be easily accomplished.

In this paper a finite element model of the structure described above is developed. Two methods for the material identification are implemented to identify a suitable material model. The work presented here is an extension of the preliminary results published in Heczko et al. (in press, 2013, 2010).

2 EXPERIMENTAL TESTING

The polyethylene foam is a cellular material that can be used for packing protection but it is also known for its several other useful properties. In order to integrate an inherent bistable element in polyethylene sheets, additional semi-circumferential cuts were introduced. Apart from the additional cuts, this structure does not need any special manufacturing technique. The base material is easily accessible and cheap. The sheets formed by two light polyethylene foam plates of density 20kg/m^3 glued together were provided by 100metros company (www.100metros.pt). The original sheet size was approximately 260x260x20-23mm.

Complete structure with bistable elements is shown in Figure 1, but for preliminary testing only a sheet with two basic cells was examined. Figure 2 gives various stages during the experiment. Unfortunately tested plates did not have the additional dense layer as the original specimen (Fig. 1b) and thus experimental results were affected by visible out-of-plane deformations. Force displacement

graph is shown in further text, together with numerical results, in Figure 4.

Figure 1. a) Complete specimen; b) detail of the composition.

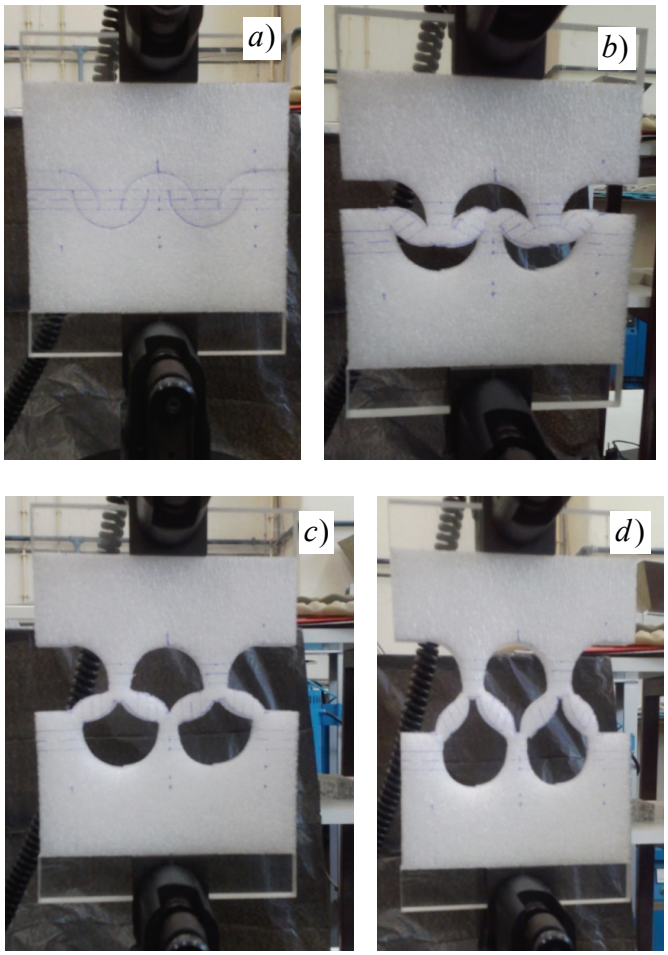

Figure 2. Tension test: a) initial position, b) onset of the negative stiffness, c) new onset of the positive stiffness, d) initiation of failure.

3 MATERIAL FITTING

This section describes how to create a finite element model. It was verified numerically that the negative branch in the force displacement graph cannot be attributed only to the geometrical non-linearity, but material properties play here a major role. Several tests on homogeneous specimens were accomplished to provide material constants characterizing the base material behaviour. It was concluded that the base material exhibits various features: (i) on one hand there is a significant orthotropy, which increases the number of parameters that are needed for the proper description; (ii) on the other hand there is a significant difference between tension and compression behaviour, namely base material is much softer in compression than in tension; and (iii) finally, the behaviour itself is strongly non-linear (Fig. 3).

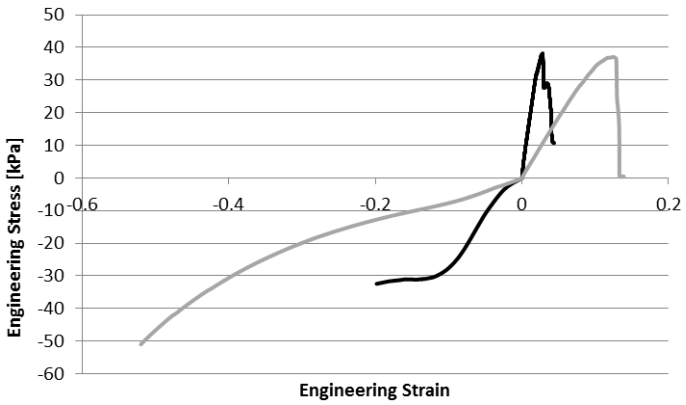

Figure 3. Tension and compression tests on homogeneous specimens (black curve – force in longitudinal direction of bubbles; grey curve – force in transversal direction of bubbles).

It is difficult to find a material model available in commercial software that would be able to account for all these features. At first, non-linearity and orthotropy were selected as the dictating matters. The results presented here were obtained in ANSYS (Release 12.1, 2009), because in ANSYS it was possible to combine elastic non-linearity (material model MELAS) with orthotropic engineering constants. Unfortunately, this non-linearity is based on von Mises stress-strain curve, i.e. without distinguishing between tension and compression behaviours. Therefore it was not adequate to use the material non-linearity obtained experimentally, because several regions of high deformations were dictated by compression and others by tension.

Regarding the orthotropy, ratio of elastic moduli between the soft and stiff direction was estimated as 4, according to the experimental tests. Since no experiments were performed to determine other properties, shear modulus was set equal to the soft Young's modulus and Poisson's ratio was estimated. Using APDL (ANSYS Parametric Design Language) an identification optimization module was

developed to fit the material data describing the physical non-linearity.

Fitting was done by a step-by-step procedure, where the slope of the stress-strain curve was tuned to achieve the expected global force. In this procedure it was important to extract maximum von Mises stress attained in Gauss integration points, to match exactly the onset of further stiffness. The corresponding total von Mises strain was calculated from the determined slope. The fitting procedure provided sufficient results, but, as expected, sometimes the slope value was not able to tune the global curve sufficiently, because the added non-linearity affected only a limited region of the finite element model.

Results presented in Figure 4 were obtained with the material constants summarized in Tables 1 and 2.

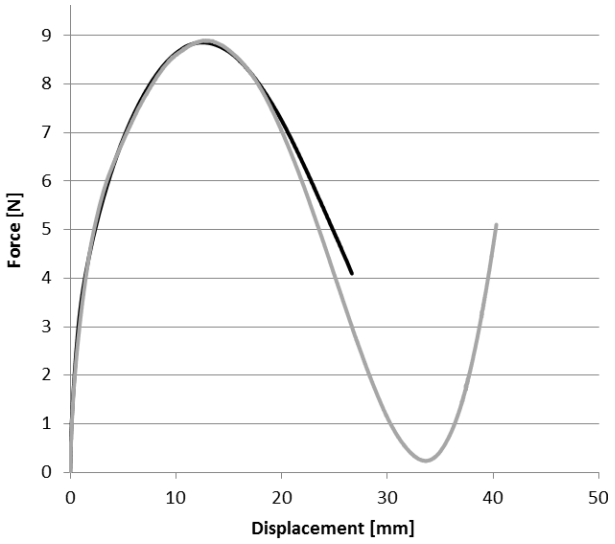

Figure 4. Comparison between experimental (grey) and numerical (black) force-displacement curves.

Table 1. Engineering constants defining the orthotropy.

E_L [MPa]	E_T [MPa]	G_{LT} [MPa]	ν_{LT}
2.25	0.55	0.55	0.3

Table 2. Values defining the elastic non-linearity.

$\varepsilon_{tot,vM}$	σ_{vM} [Pa]	E_L [MPa]
0	0	2.2
$3.2 \cdot 10^{-04}$	700	0.93
$7.5 \cdot 10^{-04}$	1100	0.39
$1.6 \cdot 10^{-02}$	7000	0.063
0.35	28000	0.034
5.35	200000	0

By analysing closely the stress strain fields at the onset of the negative stiffness, it is seen that there are only small regions of the structure that are severally compressed (Fig. 5b) and severally stretched (Fig. 5a).

It is seen from Figure 5, that apart from the global stretching, there are only very small localized regions of extreme tension and the remainder of the structure is solicited only moderately. Regarding compressions, highly compressed regions are much larger, but again, only localized regions are severely solicited. These extreme solicitations are very close to the material strength.

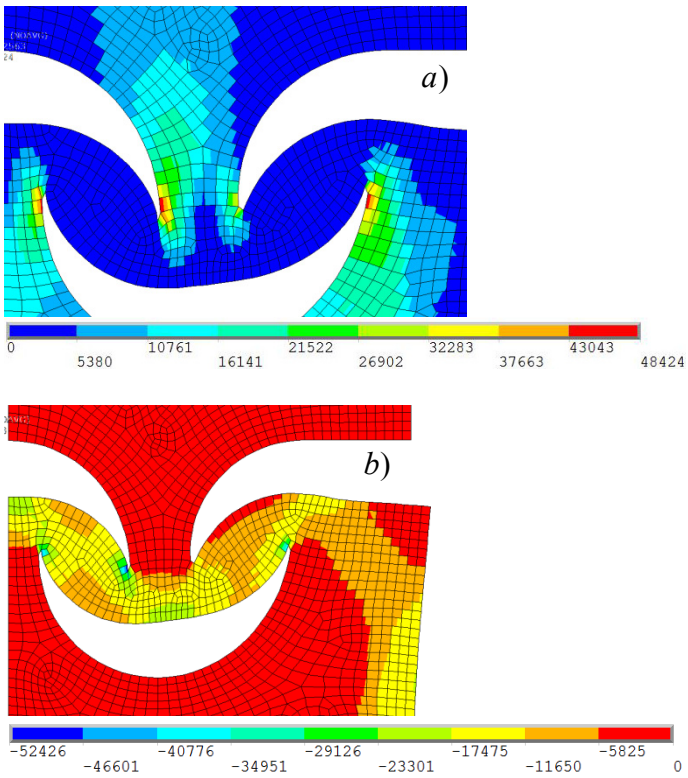

Figure 5. Principal stresses at the onset of the negative stiffness (no averaging, values from Gauss points are plotted in nodes): a) first (ranges from 0 to 48.42kPa, the legend is in Pa); b) third (ranges from 0 to -55.43kPa, the legend is in Pa).

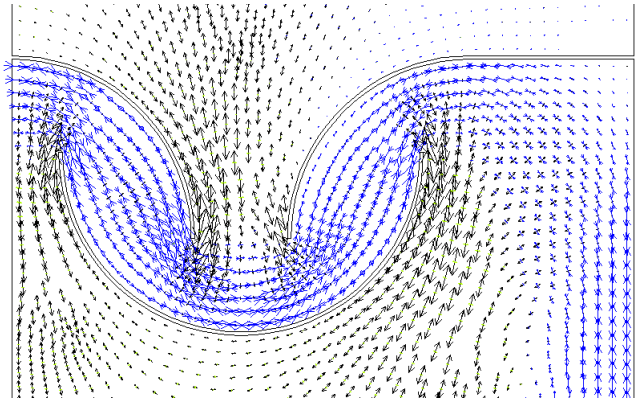

Figure 6. Principal stresses at the onset of the negative stiffness in vector plot.

Figure 6 shows maximum and minimum principal stresses with their directions, the middle principal value is perpendicular to the specimen plane. Figure 4 demonstrate that the material fitting was quite successful; nevertheless it was not possible to follow the full experimental test due to some convergence difficulties. These difficulties raise from the fact, that severe non-linearity were combined with slightly solicited regions, which can produce unphysical

deformations on the "boundary" between these regions and distort the global results. This is seen in Figure 7. At the last converged stage, the highly compressed central region did not progress smoothly and one element will revert its volume in the next solution step, due to the unphysical value of -1.97 (Fig. 7).

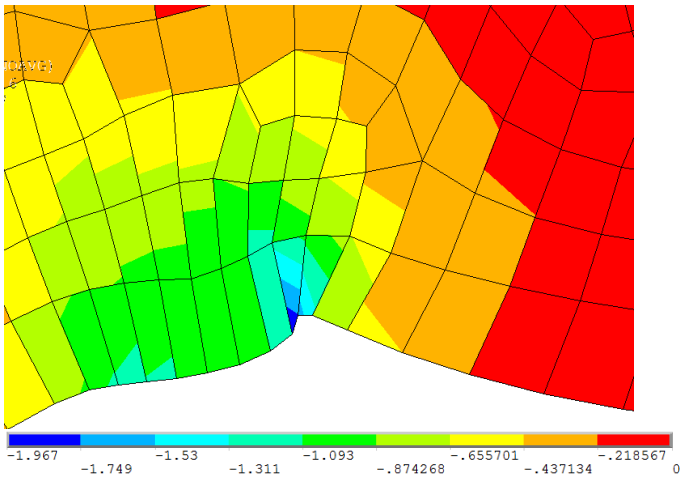

Figure 7. Third principal total strain at Gauss points at the last converged stage, the maximum compression value is -1.97.

It would be difficult to use this model for shape optimization of the inherent bistable element, because the fitting procedure already accounted for some geometrical parameters of the actual specimen and the possibility of non-convergence was not removed.

The other fitting method presented in this papers implements compressible hyperelastic materials. In such a case reversion of finite elements is removed, because, by definition, hyperelastic materials keep a positive volume for any level of compression. Numerical implementation of simple models like Neo-Hookean did not produce expected results so far, because this behaviour is generally softer in tension and stiffer in compression, on contrary to the material under consideration. The easiness of compression yielded a smooth progression along the full displacement path, and consequently did not create a necessary snap-though effect, i.e. the negative stiffness. Therefore at first, a semi-analytical material fitting is performed to match the experimental data on homogeneous specimens.

The experiments are described in terms of engineering (nominal) stress tensor and engineering strain. Therefore the material models should be optimized in this form and not in terms of the true Cauchy stress. High number of material constants is available in generalized polynomial model, with the strain energy density W is written as:

$$W = \sum_{i,j=0}^{n} C_{ij} \left(\bar{I}_1 - 3\right)^i \left(\bar{I}_2 - 3\right)^j + \sum_{k=1}^{m} D_k \left(J-1\right)^{2k}, \; C_{00} = 0 \qquad (1)$$

where n, C_{ij}, D_k are material constants, $\bar{I}_1 = J^{-2/3} I_1$, $I_1 = \lambda_1^2 + \lambda_2^2 + \lambda_3^2$, $J = \det(\mathbf{F})$, $\bar{I}_2 = J^{-4/3} I_2$, $I_2 = \lambda_1^2\lambda_2^2 + \lambda_2^2\lambda_3^2 + \lambda_3^2\lambda_1^2$ and λ_i are principal stretches defined as square roots of eigenvalues of the Left Cauchy-Green strain tensor $\mathbf{B} = \mathbf{F} \cdot \mathbf{F}^T$ and $\mathbf{F}$ is deformation gradient. In the experimental test the first Piola-Kirchoff stress components are $P_{11} \neq 0$ and $P_{22} = P_{33} = 0$. Stretches, diagonal terms of the deformation gradient $\mathbf{F}$ can be introduced for unidirectional tests as λ_1 (longitudinal) and $\lambda_2 = \lambda_3$ (transversal). Relation between λ_1 and λ_2 is obtained from the condition of the nullity of transversal stresses.

Other possibility is to use a formulation that is specifically derived for compressible forms, like Ogden-Storakes model. Following Schrodt et al. (2005), the strain energy density with a suitable volumetric function is given by:

$$W = \sum_{k=1}^{n} 2\frac{\mu_k}{\alpha_k^2}\left[\lambda_1^{\alpha_k} + \lambda_2^{\alpha_k} + \lambda_3^{\alpha_k} - 3 + \frac{1}{\beta_k}\left(J^{-\alpha_k\beta_k} - 1\right)\right] \qquad (2)$$

where α_k, β_k and μ_k are material constants. For the uniaxial tests, the longitudinal Cauchy stress is given by

$$\sigma_{11} = 2\left(\lambda_1\lambda_2^2\right)^{-1} \sum_{k=1}^{n} \frac{\mu_k}{\alpha_k}\left[\lambda_1^{\alpha_k} - \left(\lambda_1\lambda_2^2\right)^{-\alpha_k\beta_k}\right] \qquad (3)$$

and the relation between λ_1 and λ_2 is obtained from the nullity of transversal stresses

$$0 = \sum_{k=1}^{n} \frac{\mu_k}{\alpha_k}\left[\lambda_2^{\alpha_k} - \left(\lambda_1\lambda_2^2\right)^{-\alpha_k\beta_k}\right] \qquad (4)$$

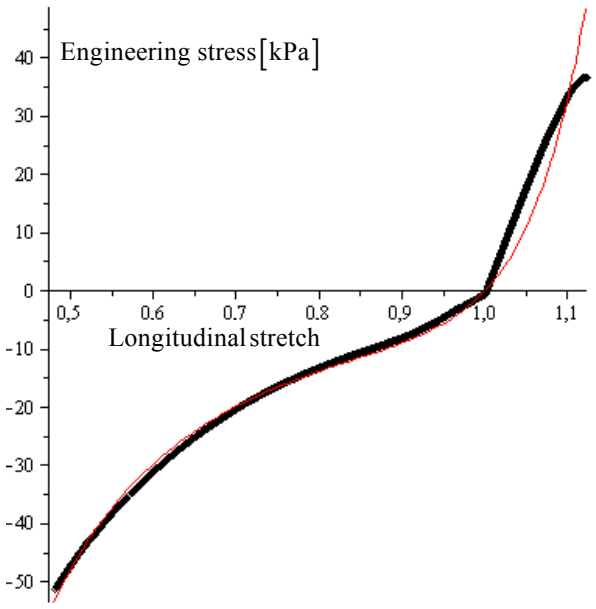

Figure 8. Fitting of Ogden-Storakes model: black dots – experimental results, thin line – analytical material curve.

For n=1 this relation can be explicitly written as

$$\lambda_2 = \lambda_1^{-\frac{\beta}{1+2\beta}} \quad (5)$$

and thus a simple parametric optimization can be accomplished.

For higher n, relation between stretches must be solved from a non-linear equation and due to a high number of material parameters optimization methods, like for instance simulated annealing, should be used. In Figure 8 result of material fitting of the softer foam direction for n=1 is shown.

The analytical material curve is obtained for $\alpha = 17.9$, $\beta = 0.11$ and $\mu = 70\text{kPa}$. It is seen that especially in compression behaviour the agreement is very good. Discrepancy in tension is caused by the discontinuity in slope of the experimental curve, which is probably originated by the fact that experiments in tension and compression were performed separately.

4 CONCLUSION

In this paper two ways of material fitting by optimization methods were implemented on a structure exhibiting a negative stiffness over a finite range of displacements during a displacement controlled tension test. Future works will address this structure shape optimization for vibration damping.

REFERENCES

Heczko J., Dimitrovová Z. & Rodrigues H.C. 2010. Optimization of linear and non-linear one-dimensional visco-elastic isolators for passive vibration control. In HC. Rodrigues, J. Herskovits, CM. Soares, JM. Guedes, J. Folgado, A. Araújo, F. Moleiro, JP. Kuzhichalil, JA. Madeira & Z. Dimitrovová (eds) *Proc. 2nd International Conference on Engineering Optimization (EngOpt2010)*, Lisbon, Portugal, 6-9 September.

Heczko J., Dimitrovová Z. & Rodrigues H.C. 2013. Composite material with negative stiffness inclusion for vibration damping: The effect of a nonlinear bistable element. In Z. Dimitrovová, JR. de Almeida & R. Gonçalves (eds) *Proc. 11th International Conference on Vibration Problems (ICOVP-2013)*, Lisbon, Portugal, 9-12 September.

Heczko J., Dimitrovová Z. & Rodrigues H.C. in press. Negative stiffness materials for vibration damping: a material realization of a nonlinear bistable element. *International Journal of Innovations in Materials Science and Engineering*.

Jaglinski T., Kochmann D., Stone D. & Lakes R.S. 2007. Materials with Viscoelastic Stiffness Greater than Diamond. *Science* 315(Feb.): 620-622.

Kalathur H. & Lakes R.S. 2013. Column Dampers with Negative Stiffness: High Damping at Small Amplitude. *Smart Materials and Structures* 22(8): 084013-21.

Kashdan L., Seepersad C.C., Haberman M. & Wilson P.S. 2012. Design, fabrication, and evaluation of negative stiffness elements using SLS. *Rapid Prototyping Journal* 18(3): 194 – 200, 2012.

Lakes R.S. 2001. Extreme Damping in Composite Materials with a Negative Stiffness Phase. *Physical Review Letters* 86(13): 2897-2900.

Release 12.1 Documentation for ANSYS, Swanson Analysis Systems IP, Inc., 2009.

Schrodt M., Benderoth G., Kuhhorn A. & Silber G. 2005. Hyperelastic Description of Polymer Soft Foams at Finite Deformations. *Technische Mechanik* 25(3-4): 162– 173.

www.100metros.pt/